Journal of Organometallic Chemistry 730 (2013) 20–31

Contents lists available at SciVerse ScienceDirect

Journal of Organometallic Chemistry

journal homepage: www.elsevier.com/locate/jorganchem

Tetraruthenium carbonyl complexes containing germyl and stannyl ligands from the reactions of $Ru_4(CO)_{13}(\mu\text{-}H)_2$ with $HGePh_3$ and $HSnPh_3$

Richard D. Adams*, Yuwei Kan, Vitaly Rassolov*, Qiang Zhang

Department of Chemistry and Biochemistry, University of South Carolina, Columbia, SC 29208, USA

ARTICLE INFO

Article history:
Received 16 July 2012
Received in revised form
10 August 2012
Accepted 17 August 2012

Keywords:
Ruthenium
Germanium
Tin
Ru–Ge bonding
DFT
UV–vis spectra

ABSTRACT

The compounds $Ru_4(CO)_{12}(GePh_3)_2(\mu\text{-}H)_4$, **1** and $Ru_4(CO)_{12}(SnPh_3)_2(\mu\text{-}H)_4$, **2** were obtained from the reactions of $Ru_4(CO)_{13}(\mu\text{-}H)_2$ with $HGePh_3$ and $HSnPh_3$, respectively. Both compounds contain a nearly planar butterfly structure for the four metal atoms with two $GePh_3/SnPh_3$ ligands and four bridging hydride ligands around the periphery of the cluster. When heated, **1** and **2** were converted into the complexes $Ru_4(CO)_{12}(\mu_4\text{-}EPh)_2$, **3**, E = Ge, and **4**, E = Sn, by cleavage of two phenyl groups from each of the $GePh_3$ ligands. Compounds **3** and **4** contain square planar arrangements of the four ruthenium atoms with quadruply bridging germylyne and stannylyne ligands on opposite sides of the square plane. The bonding and electronic transitions of **3** were analyzed by DFT computational analyses.

1. Introduction

Studies have shown that mixed metal cluster complexes can serve as precursors to superior bi- and multi-metallic nanoscale heterogeneous catalysts [1]. Germanium [2] and tin [1a,1b,3] are well known to serve as excellent modifiers for heterogeneous transition metal catalysts. We have been investigating the synthesis and structures of metal carbonyl cluster complexes containing phenylgermanium [4] and phenyltin [5] ligands for use as precursors to new nanoscale particles [5a] and heterogeneous catalysts when placed on supports [3q].

Polynuclear transition metal carbonyl cluster complexes containing terminally-coordinated EPh_3 ligands **A**, E = Ge or Sn, bridging EPh_2 ligands, **B**, triply-bridging EPh ligands, **C** and quadruply-bridging ligands EPh, **D** have been obtained from reactions of a variety of transition metal carbonyl cluster complexes with $HGePh_3$, Eqs. (1)–(4) [4a,6–8].

When using $HEPh_3$ as a reagent, it is not uncommon to obtain metal carbonyl products containing terminally coordinated EPh_3 ligands [9]. For example, the reaction of $Ru_3(CO)_{12}$ with $HEPh_3$ yields the product $Ru_3(CO)_9(EPh_3)_3(\mu\text{-}H)_3$, among many others, which contains three EPh_3 ligands [4c,]. When heated, $Ru_3(CO)_9(EPh_3)_3(\mu\text{-}H)_3$ eliminates one phenyl ring from each EPh_3 ligand and the three hydride ligands to form tris–germylene and tris–stannylene complex $Ru_3(CO)_9(\mu\text{-}EPh_2)_3$, Eq. (5) [4c,5b].

We recently obtained the $IrRu_3$ complex $IrRu_3(CO)_{11}(GePh_3)_3(\mu\text{-}H)_4$ from the reaction of $IrRu_3(CO)_{13}(\mu\text{-}H)$ with $HGePh_3$. When heated, $IrRu_3(CO)_{11}(GePh_3)_3(\mu\text{-}H)_4$ was converted to the compounds $IrRu_3(CO)_{10}(\mu\text{-}\eta^2\text{-}C_6H_5)(\mu_4\text{-}GePh)_2$ and $IrRu_3(CO)_9(\mu\text{-}\eta^2\text{-}C_6H_5)(\mu_4\text{-}GePh)_2(\mu\text{-}GePh_2)$, Eq. (6) [9]. These products contain quadruply-bridging germylyne ligands formed by cleavage of the phenyl groups from the $GePh_3$ ligands. Each product also contains one of the cleaved phenyl rings that serves as a bridging $\mu\text{-}\eta^2\text{-}C_6H_5$ ligand.

Recently, it has been shown by a computational analysis that the α-cleavage of a phenyl group from a $GePh_3$ ligand in the transformation of the triiridium complex $Ir_3(CO)_6(\mu\text{-}CO)(\mu\text{-}GePh_2)_2(GePh_3)_3$ into the complex $Ir_3(CO)_6(\eta^1\text{-}Ph)(\mu\text{-}GePh_2)_3(GePh_3)_2$, Eq. (7), occurs at a single iridium atom [10].

We have recently obtained a series of tetraruthenium complexes containing both edge-bridging EPh_2 ligands and quadruply bridging EPh ligands, E = Ge or Sn, from the reactions of $Ru_4(CO)_{12}(\mu\text{-}H)_4$ with $HGePh_3$ and $HSnPh_3$, Eq. (4) [3q,4a]. No intermediates containing $GePh_3$ or $SnPh_3$ ligands were observed in these reactions. A number of cobalt complexes containing quadruply bridging germylyne ligands have been prepared by using alkylgermanes [11].

We have now investigated the reactions of $Ru_4(CO)_{13}(\mu\text{-}H)_2$ with $HGePh_3$ and $HSnPh_3$ and have obtained the new tetrahydridotetraruthenium complexes $Ru_4(CO)_{12}(EPh_3)_2(\mu\text{-}H)_4$, **1**, E = Ge,

* Corresponding authors.
E-mail address: Adamsrd@mailbox.sc.edu (R.D. Adams).

0022-328X/$ – see front matter © 2012 Elsevier B.V. All rights reserved.
http://dx.doi.org/10.1016/j.jorganchem.2012.08.021

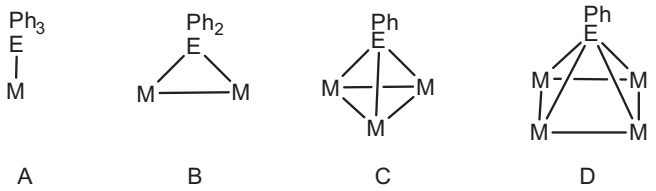

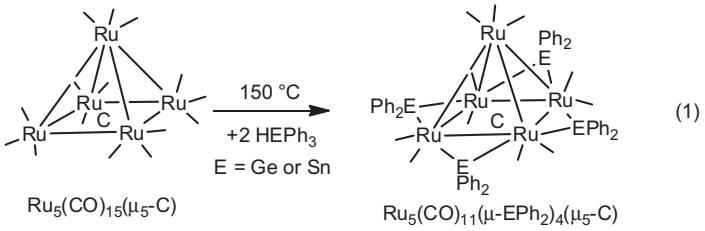

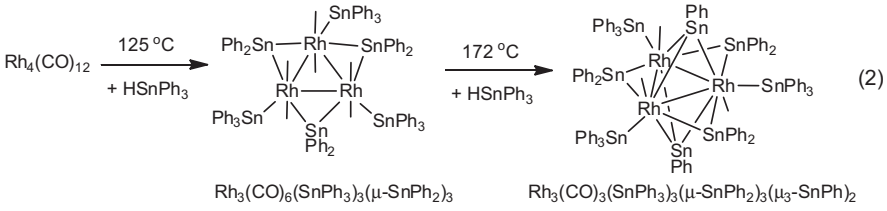

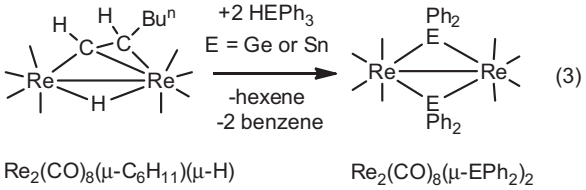

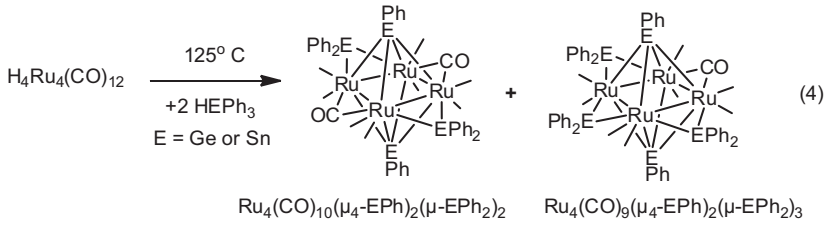

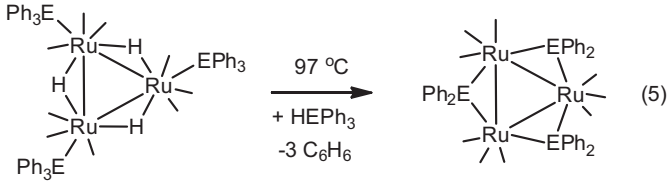

and **2**, E = Sn. When heated, **1** and **2** are converted into the complexes $Ru_4(CO)_{12}(\mu_4\text{-EPh})_2$, **3**, E = Ge, and **4**, E = Sn having quadruply bridging EPh ligands. Because of the unusual quadruply bridging coordination of the EPh groups in **3** and **4**, we have performed DFT calculations of the molecular orbitals (MOs) of **3** in order to understand the bonding of these unusual ligands to the planar Ru_4 cluster.

2. Experimental section

2.1. General data

Reagent grade solvents were dried by the standard procedures and were freshly distilled prior to use. Infrared spectra were recorded on a Thermo Nicolet Avatar 360 FT-IR spectrophotometer. ^{1}H NMR spectra were recorded on a Varian Mercury 300 spectrometer operating at 300.1 MHz. Mass spectral (MS) measurements were performed by a direct-exposure probe by

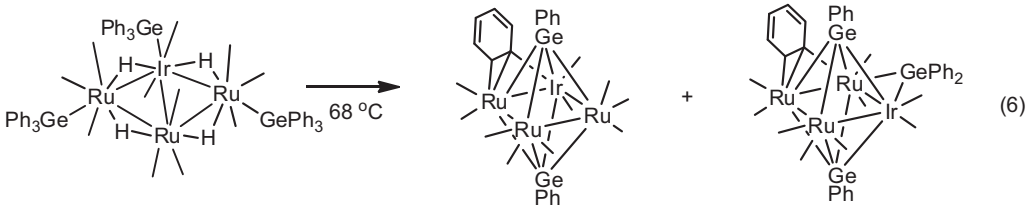

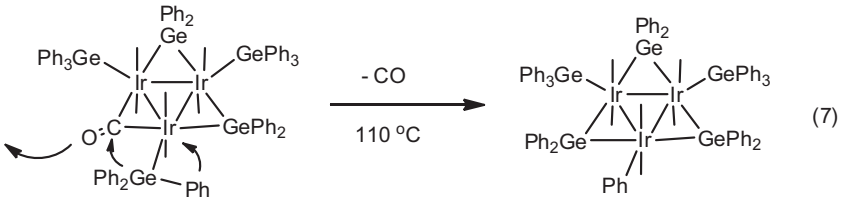

using electron impact ionization (EI) or electrospray techniques (ES) were made on a VG 70S instrument. UV–vis spectra of **3** and **4** were recorded on a Jasco V-530 UV–vis spectrometer in methylene chloride solvent at a concentration of 7.94×10^{-4} M and 1.77×10^{-3} M, respectively. $Ru_3(CO)_{12}$ was purchased from STREM. $HGePh_3$ and $HSnPh_3$ were purchased from Aldrich and were used without further purification. $Ru_4(CO)_{13}(\mu\text{-}H)_2$ was prepared according to a previously reported procedure [12]. Product separations were performed by TLC in air on Analtech 0.25 and 0.5 mm silica gel 60 Å F_{254} glass plates.

2.2. Synthesis of $Ru_4(CO)_{12}(GePh_3)_2(\mu\text{-}H)_4$, **1**

23.7 mg (0.0778 mmol) of $HGePh_3$ were added to 30.0 mg (0.0389 mmol) of $Ru_4(CO)_{13}(\mu\text{-}H)_2$ in 30 mL of hexane solvent. The reaction solution was stirred at room temperature for 6 h. An additional 6.0 mg (0.0197 mmol) of $HGePh_3$ were added to the reaction mixture six times at 3 h intervals. The color of the solution changed from red to dark orange. After the IR spectrum showed that all of the $Ru_4(CO)_{13}(\mu\text{-}H)_2$ had been consumed, the solvent was removed in vacuo. The residue was then extracted with methylene chloride, transferred to silica TLC plates and then separated by using a 6:1 hexane/methylene chloride solvent mixture to yield in order of elution: 2.5 mg of yellow $Ru_4(CO)_{12}(\mu\text{-}H)_4$ (8.6% yield) and 17.9 mg of red $Ru_4(CO)_{12}(GePh_3)_2(\mu\text{-}H)_4$, **1** (34% yield). Spectral data for **1**: IR *vCO* (cm^{-1} in hexane): 2098(w), 2058(m), 2046(vs), 2023(w), 2008(w), 1998(vw). ^1H NMR (CD_2Cl_2, in ppm) at 25 °C: δ = 7.18–7.46 (m, 30H, Ph), −15.10 (d, J_{H-H} = 12 Hz, 2H, hydride), −16.15 (d, J_{H-H} = 12 Hz, 2H, hydride). Negative ion ES/MS *m/z* 1352, $M^+ - CO$; 1324, $M^+ - CO - GePh_3$; 1020.

2.3. Synthesis of $Ru_4(CO)_{12}(SnPh_3)_2(\mu\text{-}H)_4$, **2**

18.9 mg (0.0540 mmol) of $HSnPh_3$ were added to 20.0 mg (0.0259 mmol) of $Ru_4(CO)_{13}(\mu\text{-}H)_2$ in 30 mL of hexane. The reaction solution was stirred at room temperature for 6 h. An additional 5.0 mg (0.0142 mmol) of $HSnPh_3$ were added to the reaction mixture six times at 3 h intervals. The color of the solution changed from red to a dark orange. After the IR spectrum showed that all of the $Ru_4(CO)_{13}(\mu\text{-}H)_2$ had been consumed, the solvent was removed in vacuo. The residue was then extracted with methylene chloride, transferred to silica TLC plates and then separated by using a 6:1 hexane/methylene chloride solvent mixture to yield in order of elution: 1.3 mg of yellow $Ru_4(CO)_{12}(\mu\text{-}H)_4$, (6.7% yield) and 10.1 mg of red $Ru_4(CO)_{12}(SnPh_3)_2(\mu\text{-}H)_4$, **2** (27% yield). Spectral data for **2**. IR *vCO* (cm^{-1} in hexane): 2092(w), 2059(m), 2043(vs), 2031(m), 2020(w), 2009(vw). ^1H NMR (CD_2Cl_2, in ppm) at 25 °C: δ = 7.10–7.54(m, 30H, Ph), −14.54 (d, J_{H-H} = 11 Hz, 2H, hydride), −16.22 (d, J_{H-H} = 11 Hz, 2H, hydride). Negative ion ES/MS *m/z* 1444, $M^+ - CO$; 1416, $M^+ - CO - SnPh_3$; 1066.

2.4. Synthesis of $Ru_4(CO)_{12}(\mu_4\text{-}GePh)_2$, **3**

24.7 mg (0.0183 mmol) of **1** was dissolved in hexane and heated to reflux for 1 h. The solvent was then removed in vacuo, and the residue was extracted by methylene chloride and separated by TLC using a 6:1 hexane/methylene chloride solvent mixture to yield in order of elution 1.3 mg of green $Ru_4(CO)_{12}(\mu_4\text{-}GePh)_2$, **3** (7% yield), 1.7 mg of the previously reported orange compound $Ru_3(CO)_{10}(\mu\text{-}GePh_2)_2$ (7% yield) [4c], 2.9 mg of the previously reported pale yellow compound *trans*-$Ru(CO)_4(GePh_3)_2$ (5% yield) [4c], and 0.4 mg of the previously reported purple compound $Ru_4(CO)_8(\mu\text{-}CO)_2(\mu_4\text{-}GePh)_2(\mu\text{-}GePh_2)_2$ (1.5% yield) [4a]. Spectral data for **3**. IR *vCO* (cm^{-1} in hexane): 2052(vs), 2013(s). The UV–vis absorption spectrum of **3** in CH_2Cl_2 solvent shows two broad absorptions in the visible region of the spectrum, λ_{max} = 453 nm, ε = 974 cm^{-1} M^{-1}, λ_{max} = 667 nm, ε = 893 cm^{-1} M^{-1}. Mass Spec. EI/MS, *m/z* 1040, M^+.

2.5. Synthesis of $Ru_4(CO)_{12}(\mu_4\text{-}SnPh)_2$, **4**

55 mg (0.0381 mmol) of **2** was dissolved in hexane and heated to reflux for 40 min. The solvent was then removed in vacuo, and the residue was extracted by methylene chloride and separated by TLC by using a 6:1 hexane/methylene chloride solvent mixture to yield in order of elution 1.3 mg of purple $Ru_4(CO)_{12}(\mu_4\text{-}SnPh)_2$, **4** (3% yield) [3q]; 7.9 mg of the previously reported yellow compounds $Ru_3(CO)_9(\mu\text{-}SnPh_2)_3$ (11% yield) [13], and $Ru_3(CO)_9(SnPh_3)_3(\mu\text{-}H)_3$ (17% yield) [5b]. The UV–vis absorption spectrum of **4** in CH_2Cl_2

Table 1
Crystallographic data for compounds **1**–**3**.

Compound	**1**	**2**	**3**
Empirical formula	$Ru_4Ge_2O_{12}C_{48}H_{34}\cdot CH_2Cl_2$	$Ru_4Sn_2O_{12}C_{48}H_{34}\cdot CH_2Cl_2$	$Ru_4Ge_2O_{24}C_{12}H_{10}$
Formula weight	1437.14	1529.34	1039.78
Crystal system	Orthorhombic	Orthorhombic	Triclinic
Lattice parameters			
a (Å)	27.782(5)	28.239(3)	9.1544(3)
b (Å)	11.652(2)	11.8678(14)	9.6436(4)
c (Å)	16.575(3)	16.6154(19)	9.7194(4)
α (°)	90.00	90.00	73.303(1)
β (°)	90.00	90.00	83.863(1)
γ (°)	90.00	90.00	65.546(1)
V (Å^3)	5365.4(16)	5568.5(11)	748.07(5)
Space group	*P*bcn(#60)	*P*bcn(#60)	*P*-1(#2)
Z	4	4	1
ρ_{calc} (g/cm^3)	1.78	1.82	2.31
μ (Mo Kα) (mm^{-1})	2.360	2.091	4.009
Temperature (K)	294(2)	294(2)	293(2)
$2\Theta_{max}$ (°)	41.50	33.14	50.04
No. obs. ($I > 2\sigma(I)$)	3019	4918	2642
No. parameters	310	306	190
Goodness of fit (GOF)	1.025	1.037	1.049
Max. shift in final cycle	0.001	0.001	0.001
Residuals[a]: *R*1; *wR*2	0.0573; 0.0993	0.0598; 0.0964	0.0345; 0.1018
Absorption correction, max/min	Multi-scan 1.000/0.303	Multi-scan 1.000/0.380	Multi-scan 1.000/0.653
Largest peak in final diff. map (e$^-$/Å^3)	0.715	0.678	1.789

[a] $R = \sum_{hkl}(||F_{obs}| - |.F_{calc}|.|)/\sum_{hkl}|F_{obs}|$; $R_w = [\sum_{hkl}w(|F_{obs}| - |.F_{calc}|.)^2/\sum_{hkl}wF_{obs}^2]^{1/2}$; $w = 1/\sigma^2(F_{obs})$; GOF $= [\sum_{hkl}w(|F_{obs}| - |.F_{calc}|.)^2/(n_{data} - n_{vari})]^{1/2}$.

solvent shows two broad absorptions in the visible region of the spectrum, λ_{max} = 530 nm, ε = 245 cm^{-1} M^{-1}, λ_{max} = 680 nm, ε = 153 cm^{-1} M^{-1}.

2.6. Crystallographic analyses

Red crystals of **1** and **2** suitable for X-ray diffraction analyses were obtained by slow evaporation of solvent from solutions of the pure compound in a hexane/methylene chloride solvent mixture at room temperature. Dark purple single crystals of **3** suitable for X-ray diffraction analyses were obtained by slow evaporation of solvent from a hexane/methylene chloride solvent at −30 °C. Each data crystal was glued onto the end of a thin glass fiber. X-ray diffraction intensity data were measured by using a Bruker SMART APEX CCD-based diffractometer using Mo Kα radiation (λ = 0.71073 Å). The raw data frames were integrated with the SAINT+ program by using a narrow-frame integration algorithm [14]. Corrections for Lorentz and polarization effects were also applied with SAINT+. An empirical absorption correction based on the multiple measurement of equivalent reflections was applied using the program SADABS [14]. All structures were solved by a combination of direct methods and difference Fourier syntheses, and refined by full-matrix least-squares on F^2 by using the SHELXTL software package [15]. All non-hydrogen atoms were refined with anisotropic thermal parameters. Hydrogen atoms on the phenyl rings were placed in geometrically idealized positions and included as standard riding atoms during the least-squares refinements. Compounds **1** and **2** are isomorphous. They crystallized in the orthorhombic crystal system.

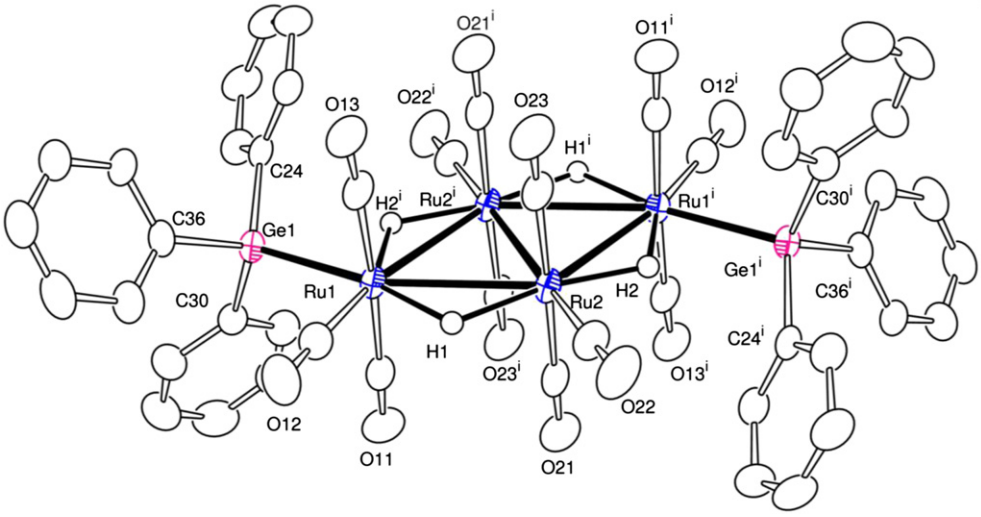

Fig. 1. An ORTEP diagram of $Ru_4(CO)_{12}(GePh_3)_2(\mu\text{-}H)_4$, **1** showing 30% probability thermal ellipsoids. The hydrogen atoms on phenyl groups are omitted for clarity. Selected bond distances (in Å) are as follow: Ru(1)–Ru(2) = 3.0734(9), Ru(1)–Ru(2^i) = 3.0130(9), Ru(2)–Ru(2^i) = 2.8744(12), Ru(1)–Ge(1) = 2.5501(10), Ru(1)–H(1) = 1.98(8), Ru(1)–H(2) = 1.81(5), Ru(2)–H(1) = 1.94(8), Ru(2)–H(2) = 1.75(5).

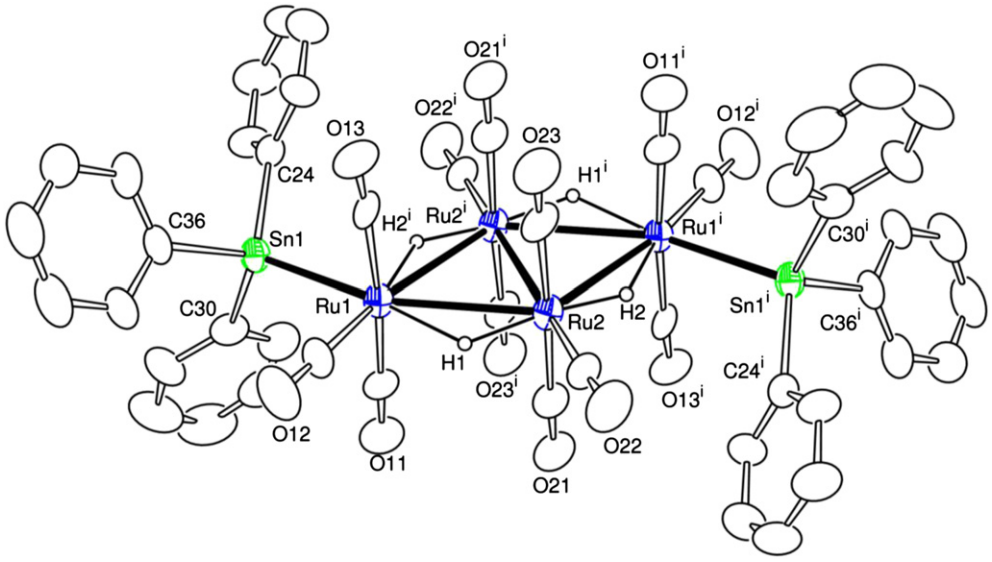

Fig. 2. An ORTEP diagram of $Ru_4(CO)_{12}(SnPh_3)_2(\mu\text{-}H)_4$, **2** showing 20% probability thermal ellipsoids. The hydrogen atoms on phenyl groups are omitted for clarity. Selected bond distances (in Å) and angles in (°) are as follow: Ru(1)–Ru(2) = 3.0434(12), Ru(1)–Ru(2^i) = 3.0031(13), Ru(2)–Ru(2^i) = 2.8796(16), Ru(1)–Sn(1) = 2.6894(11), Ru(1)–H(1) = 1.88(8), Ru(1)–H(2) = 1.84(9), Ru(2)–H(1) = 1.58(8), Ru(2)–H(2) = 1.48(9), Sn(1)–Ru(1)–Ru(2) = 157.73(4).

The space group *P*bcn was established by the pattern of systematic absences observed in the data and was confirmed by the successful solution and refinement of the structure in both cases. The hydride ligands in compounds **1** and **2** were located, and refined without restraints by using isotropic thermal parameters. Compound **3** crystallized in the triclinic system. The space group $P\bar{1}$ was assumed and confirmed by the successful solution and refinement for the structure. Crystal data, data collection parameters, and results of the analyses are listed in Table 1.

3. Computational details

All density functional theory (DFT) calculations were performed with the ADF suite of programs [16a–b] using the PBEsol functional [16c] with Slater-type triple-zeta polarized TZP basis sets with small frozen cores, and scalar relativistic correction. We performed an extensive study of various functionals (B3LYP, M06 family, TPSS family, PBE family) and all-electron vs. frozen core basis sets, and the chosen model provides an optimum compromise between the accuracy and the computational cost, although we found that it is necessary to increase the default numerical integration accuracy parameter to 6. The geometric structure of **3** was optimized as gas-phase with point symmetric group of C_{2h}. The time-dependent DFT (TDDFT) calculation was performed at the same theory level. The transitions to triplet and higher order multiplet excited states from the ground state are forbidden because the ground states of the species in this study are singlets. Even if some of these forbidden transitions gain intensity by spin-orbit splitting, their intensities in absorption spectrum should still be very weak relative to the transitions to the singlet excited states.

4. Results and discussion

The compounds $Ru_4(CO)_{12}(GePh_3)_2(\mu\text{-}H)_4$, **1** (34% yield) and $Ru_4(CO)_{12}(SnPh_3)_2(\mu\text{-}H)_4$, **2** (27% yield) were obtained from the reactions of $Ru_4(CO)_{13}(\mu\text{-}H)_2$ with $HGePh_3$ and $HSnPh_3$, respectively. Compounds **1** and **2** were both characterized by a combination of IR, ^1H NMR and single-crystal X-ray diffraction analyses. Compounds **1** and **2** are isomorphous and crystallized in the orthorhombic crystal system. Both compounds are structurally similar. ORTEP diagrams of the molecular structure of **1** and **2** are shown in Figs. 1 and 2, respectively. Both compounds consist of a butterfly cluster of four ruthenium atoms. In the solid

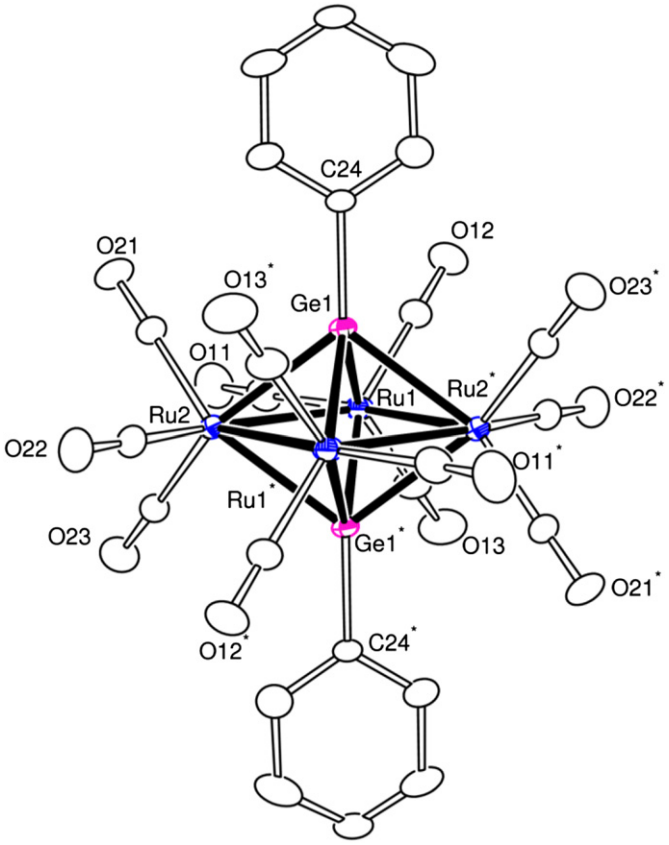

Fig. 3. An ORTEP diagram of $Ru_4(CO)_{12}(\mu_4\text{-}GePh)_2$, **3** showing 20% probability thermal ellipsoids. The hydrogen atoms are omitted for clarity. Selected bond distances (in Å) are as follow: Ru(1)–Ru(2) = 2.8830(4), Ru(2)–Ru(1*) = 2.8850(3), Ru(1)–Ge(1) = 2.5586(3), Ru(2)–Ge(1) = 2.5559(4), Ru(1)–Ge(1′) = 2.5576(4), Ru(2)–Ge(1′) = 2.5573(4), Ge(1)–C(24) = 1.944(3).

state the molecule sits on a center of symmetry and the cluster of four ruthenium atoms is thus planar in the solid state. Both molecules are similar to the planar $IrRu_3$ cluster complex $IrRu_3(CO)_{11}(GePh_3)_3(\mu\text{-}H)_4$, **5** that was obtained from the reaction of $IrRu_3(CO)_{13}(\mu\text{-}H)$ with $HGePh_3$ [9]. Compound **5** differs from **1** by the replacement of one of the hinge-positioned $Ru(CO)_3$ groups with an $Ir(CO)_2(GePh_3)$ group.

There are five Ru–Ru bonds in each molecule, only three

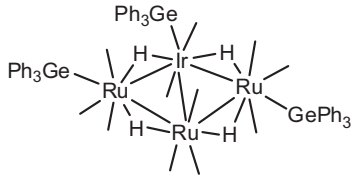

5

are symmetry independent: for **1**: Ru(1)–Ru(2) = 3.0734(9) Å, Ru(1)–Ru(2^i) = 3.0130(9) Å, Ru(2)–Ru(2^i) = 2.8744(12) Å; for **2**: Ru(1)–Ru(2) = 3.0434(12) Å, Ru(1)–Ru(2^i) = 3.0031(13) Å, Ru(2)–Ru(2^i) = 2.8796(16) Å. The Ru–Ru bond distances in **5** have similar lengths: Ru(1)–Ru(2) = 3.0305(9) Å, Ru(2)–Ru(3) = 3.0316(9) Å. Each of the peripheral Ru–Ru bonds in **1** and **2** contains a bridging hydride ligand that was located and refined crystallographically. They exist as two inequivalent pairs and thus exhibit two resonances in the ^1H NMR spectrum: for **1**: $\delta = -15.10$ (d, $J_{H-H} = 12$ Hz), -16.15 (d, $J_{H-H} = 12$ Hz); for **2**: $\delta = -14.54$ (d, $J_{H-H} = 11$ Hz), -16.22 (d, $J_{H-H} = 11$ Hz). As expected, the hydride-bridged Ru–Ru bonds are significantly longer than the diagonal hinge Ru–Ru bond [17a].

Each ruthenium atom contains three linear terminal carbonyl ligands. The two wing-tip Ru atoms, Ru(1) and Ru(1^i), also contain an additional EPh_3 ligand, E = Ge or Sn, that lies in the plane of the cluster in the position trans to the Ru(1)–Ru(2) bond, for **1**: Ru(1)–Ge(1) = 2.5501(10) Å, Ru(2)–Ru(1)–Ge(1) = 157.94(3)°, for **2**: Ru(1)–Sn(1) = 2.6894(11), Ru(2)–Ru(1)–Sn(1) = 157.73(4)°. The Ru–Ge bond distances in **1** are very similar to those in **5**: Ru(1)–Ge(2) = 2.5430(9) Å, Ru(3)–Ge(3) = 2.5431(9) Å.

When a solution of **1** was heated to reflux for 1 h in a hexane solution, it was converted into the new compound $Ru_4(CO)_{12}(\mu_4\text{-}GePh)_2$, **3** in 7% yield. Several previously reported coproducts: $Ru_3(CO)_{10}(\mu\text{-}GePh_2)_2$ (7% yield) [4c], *trans*-$Ru(CO)_4(GePh_3)_2$ (5% yield) [4c], and $Ru_4(CO)_8(\mu\text{-}CO)_2(\mu_4\text{-}GePh)_2(\mu\text{-}GePh_2)_2$, **6** (1.5% yield) [4a] were also obtained. Compound **3** was

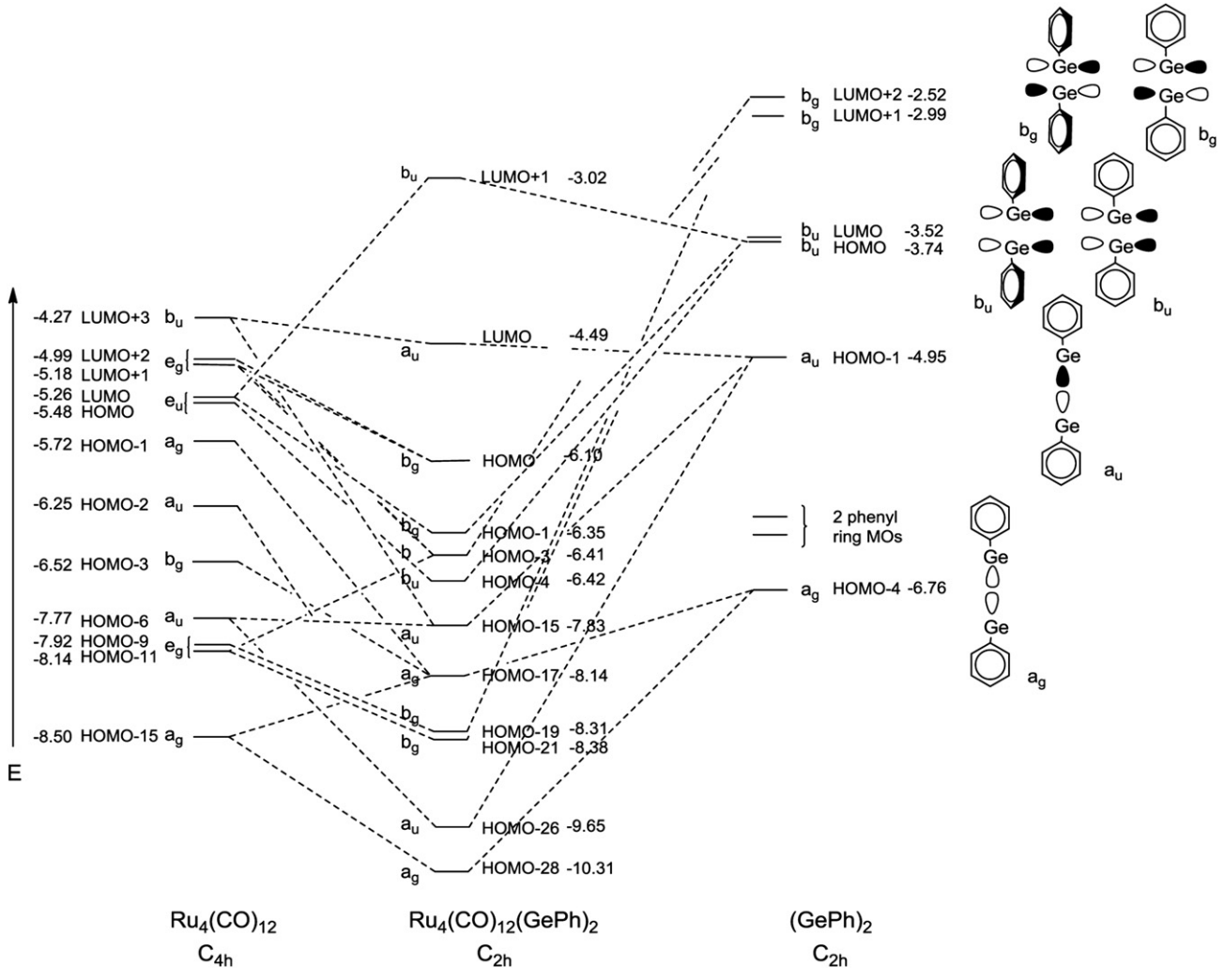

Fig. 4. A molecular orbital energy level diagram in eV for compound **3** and selected molecular fragments. The symmetry correlations $C_{4h} \rightarrow C_{2h}$ are as follow: $a_g \rightarrow a_g$, $b_g \rightarrow a_g$, $e_g \rightarrow 2b_g$, $a_u \rightarrow a_u$, $b_u \rightarrow a_u$, $e_u \rightarrow 2b_u$.

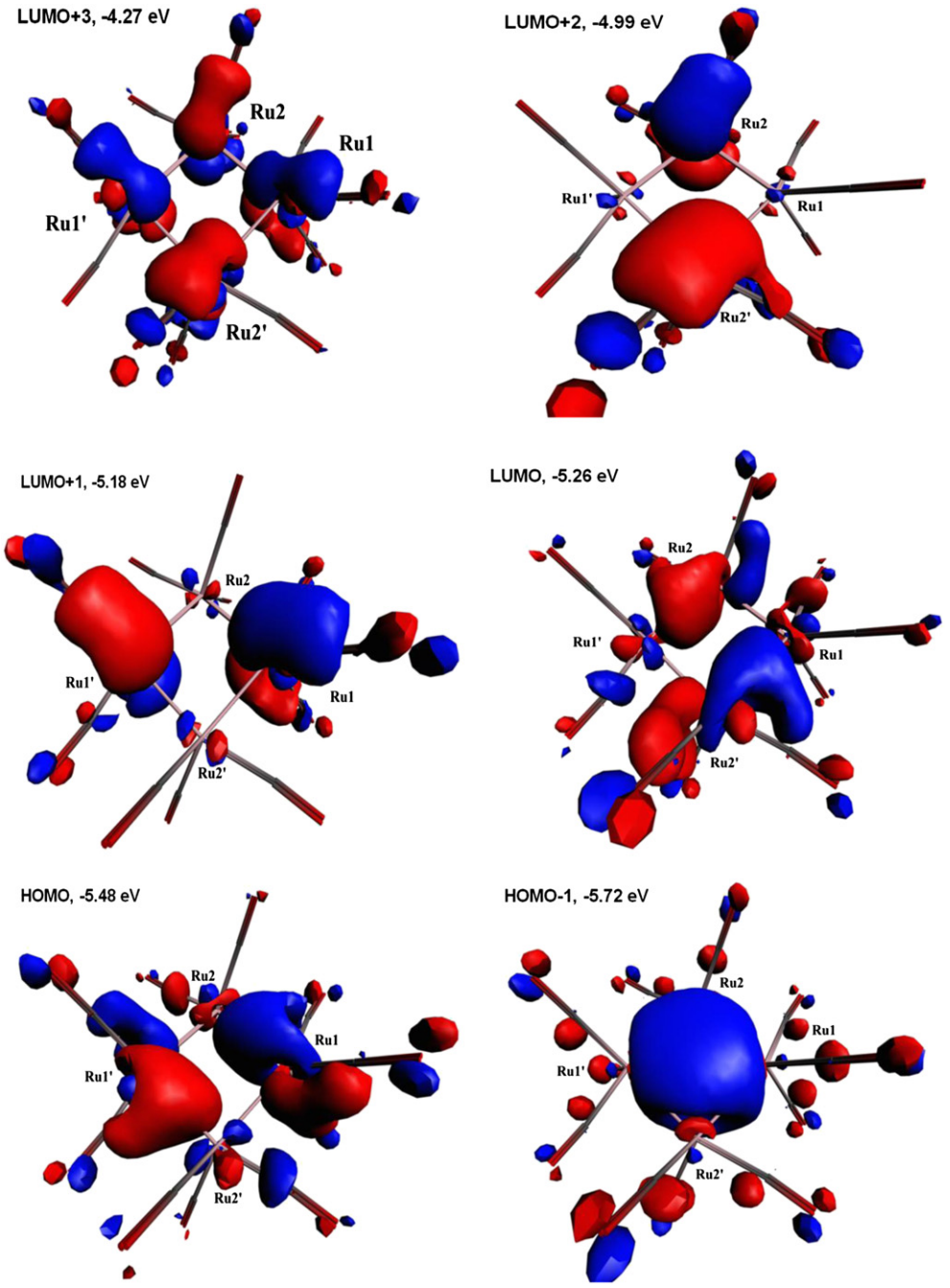

Fig. 5. Selected molecular orbitals for the $Ru_4(CO)_{12}$ fragment of compound **3**.

characterized by IR spectroscopy, ν(CO), 2052 cm^{-1}, 2013 cm^{-1}, UV–vis spectroscopy, mass spectrometry and single-crystal X-ray diffraction analyses.

An ORTEP diagram of the molecular structure of **3** is shown in Fig. 3. In the solid state the molecule sits on a center of symmetry and is thus crystallographically centrosymmetric. The cluster contains four ruthenium atoms in a square planar arrangement. The two independent Ru–Ru distances are equivalent within experimental error, Ru(1)–Ru(2) = 2.8830(4) Å, Ru(2)–Ru(1*) = 2.8850(3) Å. There are two quadruply bridging GePh ligands that lie on each side of the Ru_4 plane. These distances are shorter than the $GePh_2$ bridged Ru–Ru bond distance in **6**, 2.9508(9) Å, and longer than the CO-bridged Ru–Ru bond in **6**, 2.8188(7) Å [4a].

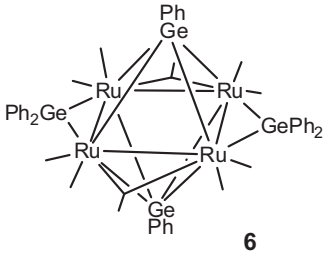

6

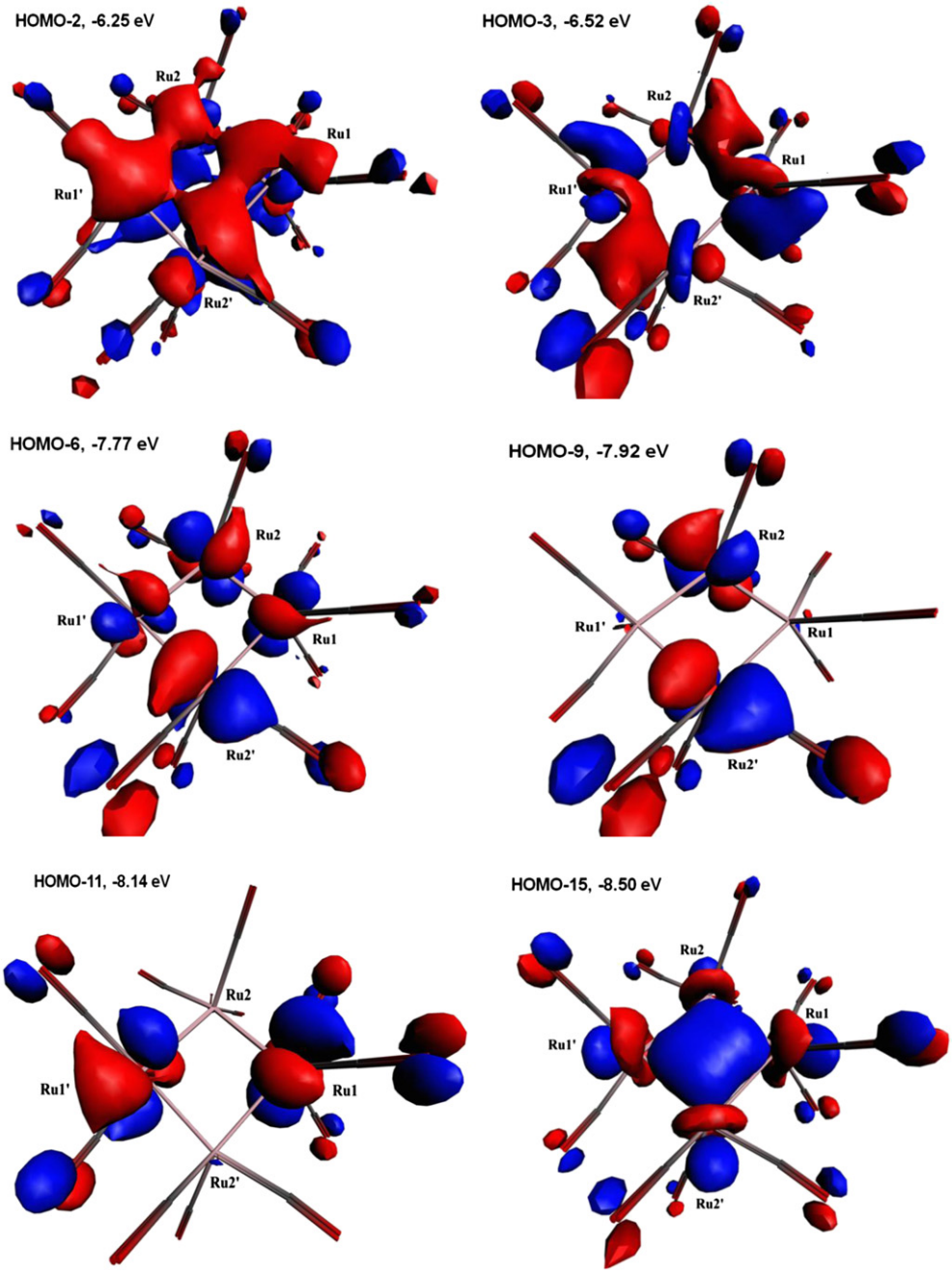

Fig. 5. (*continued*).

The four independent Ru–Ge distances are not significantly different: Ru(1)–Ge(1) = 2.5586(3) Å, Ru(2)–Ge(1) = 2.5559(4) Å, Ru(1)–Ge(1′) = 2.5571(6) Å, Ru(2)–Ge(1′) = 2.5563(6) Å and they are very similar to the Ru–Ge distances to the quadruply-bridging GePh ligands in **6**: 2.5497(10) Å, 2.5565(10) Å and 2.5580(8) Å. The Ge–C distance to the phenyl ring, Ge(1)–C(24) = 1.944(3) Å in **3** is the same as that found for the Ge–C distance for the quadruply bridging GePh ligand in **6**, 1.940(7) Å. Each Ru atom contains three linear carbonyl ligands. One CO ligand lies in the Ru_4 plane. The other two lie symmetrically on either side of the Ru_4 plane such that the molecule overall has an approximate C_{4h} symmetry.

When heated to reflux in hexane solvent, compound **2** was converted into the previously reported compound $Ru_4(CO)_{12}(\mu_4\text{-}SnPh)_2$, **4** but the yield was very low (3%) [3q]. Two other previously reported compounds $Ru_3(CO)_9(\mu\text{-}SnPh_2)_3$ (11% yield) [12] and $Ru_3(CO)_9(SnPh_3)_3(\mu\text{-}H)_3$ (17% yield) [5b] were also obtained. Compound **4** is structurally similar to **3**.

The bonding of the GePh and SnPh ligands to the $Ru_4(CO)_{12}$ cluster is somewhat unconventional because the Ge/Sn atoms are each bonded to five atoms: the four Ru atoms and one carbon atom of its attached phenyl ring. Square planar, tetranuclear transition metal cluster complexes can be viewed as having four metal–metal bonds. When the metal atoms in these complexes obey the 18-electron rule, the metal atoms generally have a total of 64 valence electrons [18]. However, there are a number of examples of square planar, tetranuclear transition metal cluster complexes containing bridging ligands that have only 62 valence electrons [19]. Compound **3** belongs to the family of 62 valence

electron tetranuclear metal complexes and is "formally" electron deficient.

In order to understand the bonding of the quadruply-bridging GePh and SnPh ligands to the four metal atoms in **3**, DFT molecular orbitals were calculated by using the PBEsol functional of the ADF library [16]. To explain the bonding in compound **3** we will consider the molecule as a combination of two face to face GePh fragments interacting with a square planar $Ru_4(CO)_{12}$. The $Ru_4(CO)_{12}$ fragment has approximate C_{4h} symmetry. If one includes the eclipsed phenyl groups on the Ge atoms, compound **3** has an

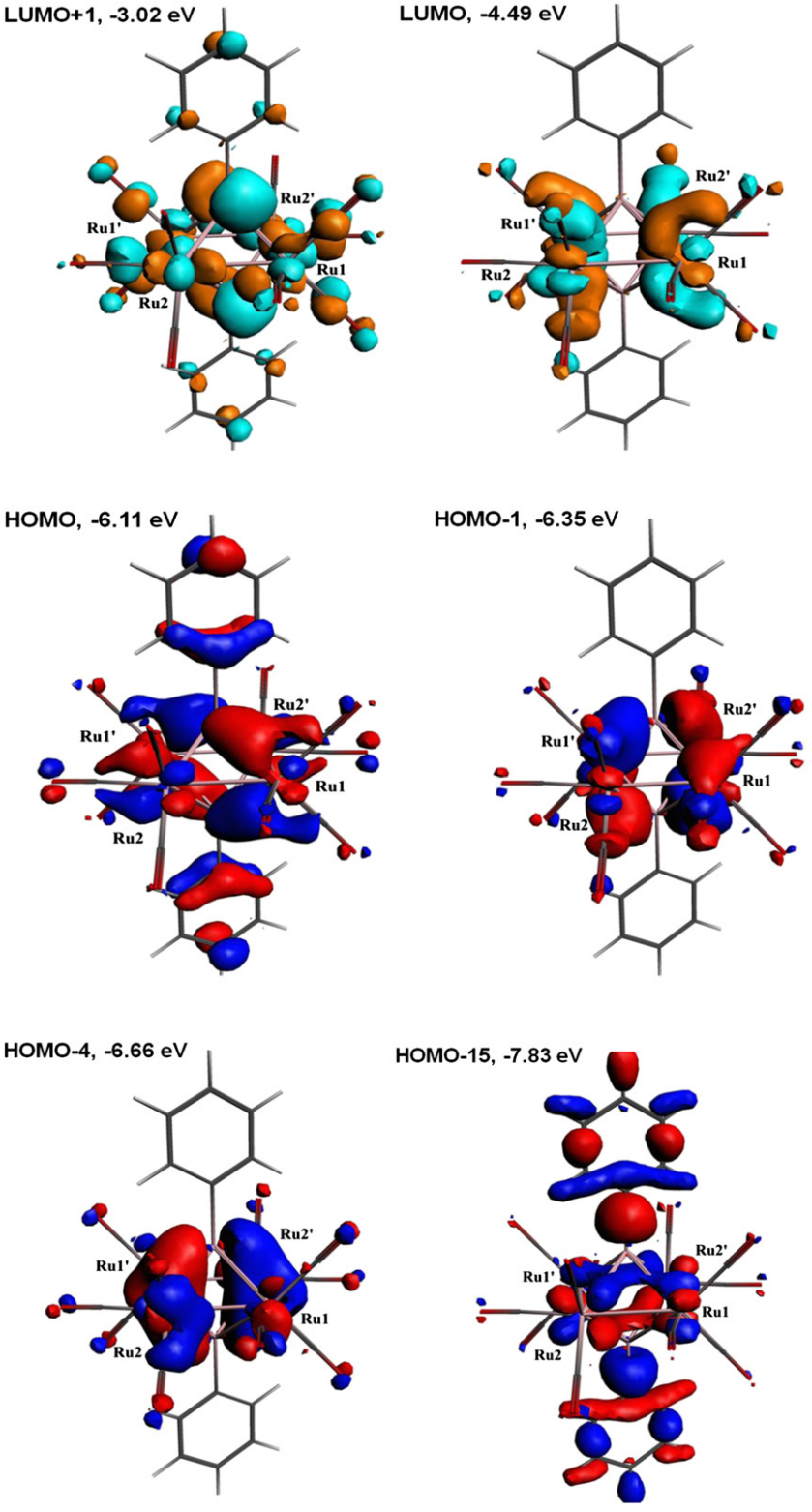

Fig. 6. Selected molecular orbitals for compound **3**.

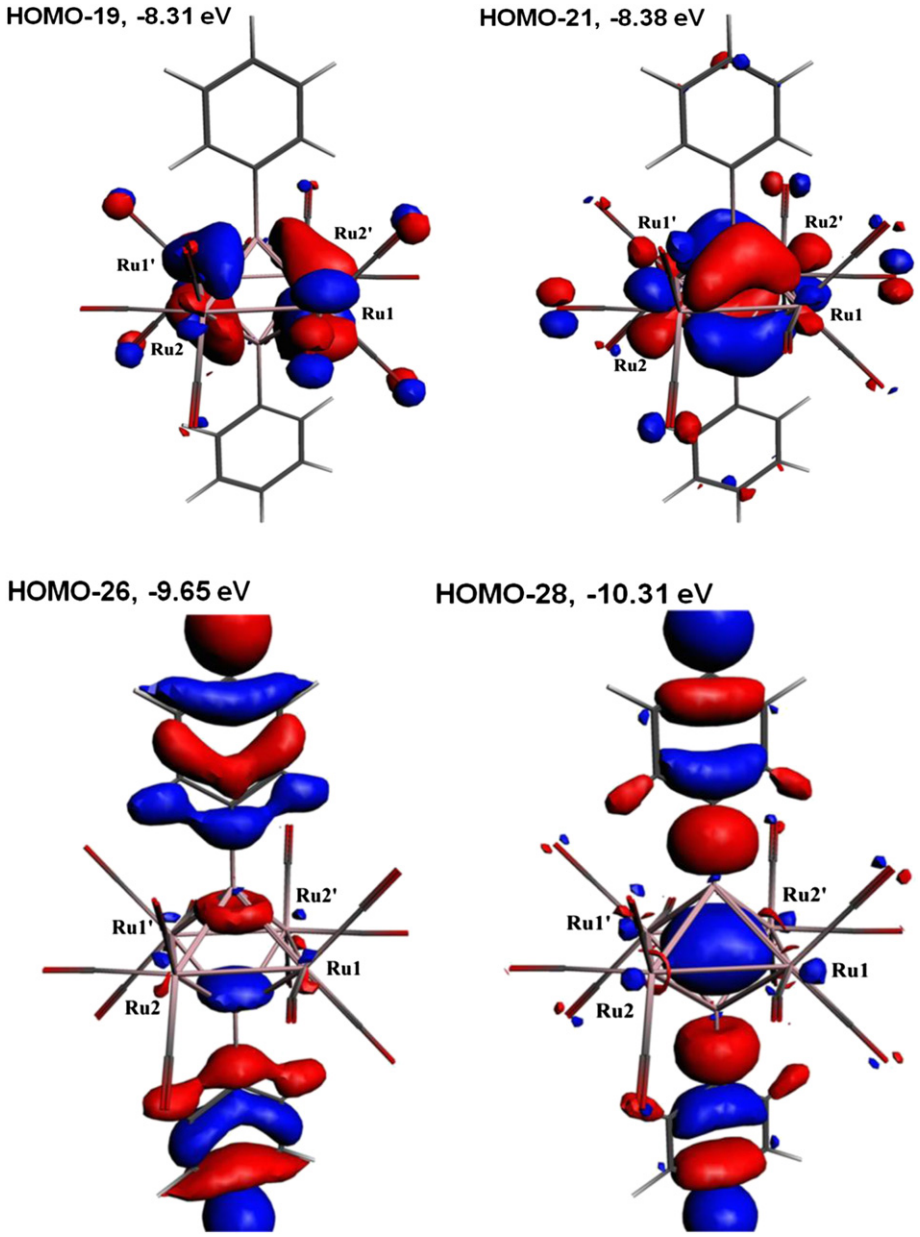

Fig. 6. (*continued*).

idealized symmetry of C_{2h}. Our DFT analysis of compound **3** was performed in the following way. The molecular orbitals and their energies were obtained from a geometry-optimized structure for **3** by starting with the positional parameters obtained from the crystal structure analysis. Molecular orbitals for the $Ru_4(CO)_{12}$ fragment were then obtained by deleting the two GePh ligands and performing a single point calculation on the remaining atoms. Molecular orbitals for the suitably-oriented GePh fragments were obtained by deleting the $Ru_4(CO)_{12}$ fragment of the optimized **3** and performing a single point calculation on the remaining atoms. A molecular energy level correlation diagram is shown in Fig. 4.

The atomic orbital (AO) combinations of the two GePh fragments that are available for bonding to the metal atoms are sketched at the far right of Fig. 4. Each GePh fragment has one orbital which can be viewed as a sp hybrid that is pointing toward the Ge atom of the other GePh fragment and also two p-orbitals that are perpendicular to the Ge—Ge vector. Symmetry assignments are based on the point group C_{2h} because of the presence of the two eclipsed phenyl rings. The calculated energies of these orbital combinations and their symmetries are shown in Fig. 4 to the left of the sketches of the two GePh fragments. The sp hybrids form a pair of orbitals; the symmetric a_g (HOMO − 4) and the antisymmetric a_u (HOMO − 1) which are interleaved by two phenyl ring orbitals. The latter are not shown because they are not important for understanding the bonding of the GePh fragments to the metal atoms. The four p-orbitals give four binary combinations: two of b_u symmetry and two of b_g symmetry. The two b_u orbitals are not equal in energy due to different interactions between them and the phenyl rings. For the same reason the two higher energy b_g orbitals are also not of equal in energy.

The energy levels of MOs for the $Ru_4(CO)_{12}$ fragment are shown on the far left of Fig. 4. Selected MOs for the $Ru_4(CO)_{12}$ fragment are

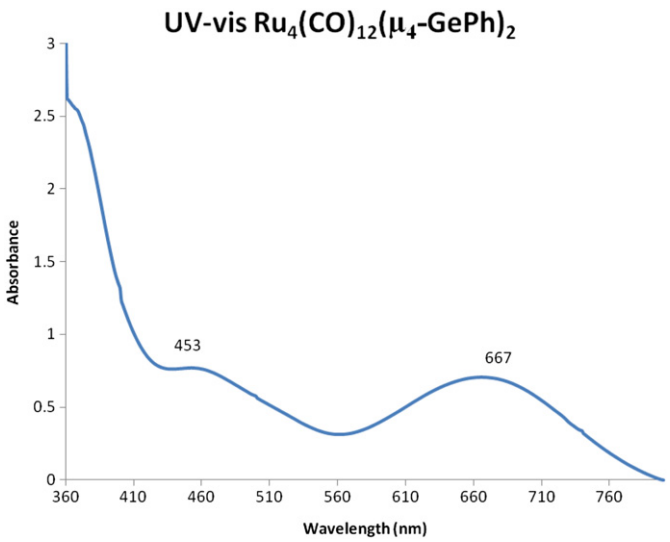

Fig. 7. UV–vis spectrum of **3** in methylene chloride solution.

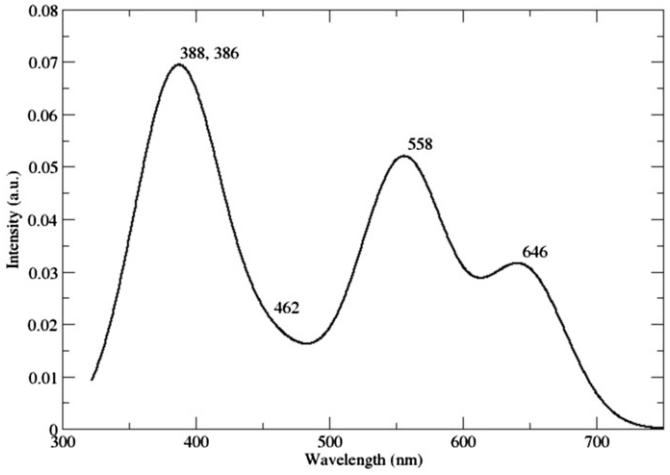

Fig. 8. TD-PBEsol calculated UV–vis spectrum of compound **3**.

shown in Fig. 5. The symmetry of these MOs has been assigned by using the idealized point group C_{4h} but the energies of the two components of the e_u and e_g orbitals are not identical because our arrangement of the atoms was not exactly according to C_{4h} symmetry.

The selected MOs for a geometry-optimized version of **3** are shown in Fig. 6. The energy and their symmetry assignments are based on idealized C_{2h} symmetry. These orbitals and their correlations to the appropriate MOs of the fragments are shown in center of Fig. 4. Note: The e_u and e_g orbitals of the $Ru_4(CO)_{12}$ fragment split and are converted into two orbitals of b_u symmetry and two orbitals of b_g symmetry, respectively, upon crossing over from the C_{4h} symmetry of the $Ru_4(CO)_{12}$ fragment to the C_{2h} symmetry of **3**, and the a_g and b_g representations of C_{4h} symmetry both become a_g in C_{2h} and the a_u and b_u orbitals both become a_u in C_{2h}. The a_g HOMO − 4 of the GePh fragments forms a strong bonding interactions to the a_g, HOMO − 1 and HOMO − 15, of the $Ru_4(CO)_{12}$ fragment to form the strongly bonding HOMO − 28 in **3**. The b_g HOMO − 3 of the $Ru_4(CO)_{12}$ fragment is predominantly metal–metal bonding and becomes the a_g HOMO − 17 in **3**, see Fig. 6. The a_u HOMO − 1 of the GePh fragments forms strong bonding interactions to the A_u HOMO − 2 and HOMO − 6 of the $Ru_4(CO)_{12}$ fragment to form the strongly bonding HOMO − 26 and the HOMO − 15 in **3**. The b_u orbitals, HOMO and LUMO, of the GePh fragments form strong bonding interactions to the e_u, HOMO and LUMO, of the $Ru_4(CO)_{12}$ fragment to form the bonding pair HOMO − 3 and HOMO − 4 and the unoccupied LUMO + 1 in **3**. The two b_g orbitals, LUMO + 1 and LUMO + 2, of the GePh fragments form bonding interactions to the e_g orbitals, LUMO + 1 and LUMO + 2, of the $Ru_4(CO)_{12}$ fragment to form the bonding pair HOMO and HOMO − 1 in **3**. They also complement the bonding pair of e_g orbitals, HOMO − 9 and HOMO − 11, of the $Ru_4(CO)_{12}$ fragment to create the strongly bonding pair of b_g orbitals, HOMO − 19 and HOMO − 21 in **3**.

A number of years ago, Halet et al. examined the bonding of the complexes of this type by extended Hückel methods [20]. Specifically, they considered the 64 electron model compound $Fe_4(CO)_{12}(\mu_4\text{-}PH)_2$, **7**. In **7** the HOMO was a b_u orbital (C_{4h} symmetry) analogous to our a_u LUMO (C_{2h} symmetry) for **3** because **7** has two more electrons that **3**. Because they are "formally" unsaturated the 62 electron cluster complexes have a smaller HOMO–LUMO gap and these compounds turn out to be highly colored. For this reason we have also measured the UV–vis absorption spectra of **3** and **4**.

Compounds **3** (blue) and **4** (purple) both exhibit two broad absorptions in the visible region: for **3**, λ_{max} = 453 nm, ε = 974 cm^{-1} M^{-1}, λ_{max} = 667 nm, ε = 893 cm^{-1} M^{-1}; for **4**, λ_{max} = 530 nm, ε = 245 cm^{-1} M^{-1}, λ_{max} = 680 nm, ε = 153 cm^{-1} M^{-1}. The observed spectrum of **3** is shown in Fig. 7.

The UV–vis absorption spectrum for **3** was calculated from our geometry-optimized structure by using a time-dependent PBEsol calculation. The computed spectrum of **3** is shown in Fig. 8. The observed absorption at 667 nm is attributed to two transitions HOMO − 1 to LUMO and HOMO to LUMO that are based in the Ru_4 core of the cluster. They are calculated to be 558 nm, f = 0.047 and 646 nm, f = 0.030, respectively. The observed absorption at 453 nm is attributed to the HOMO − 8 (π-ring atomic orbitals) to LUMO transition and is calculated to be 462 nm, f = 0.012. A high energy absorption at approx. 388 nm (calcd) is due to transitions within the phenyl rings.

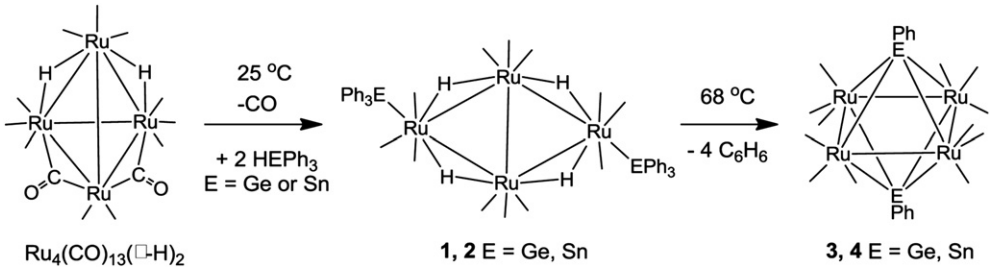

Scheme 1.

5. Summary

The new planar butterfly cluster complexes **1** and **2** have been obtained from the reactions of $Ru_4(CO)_{13}(\mu\text{-}H)_2$ with $HGePh_3$ and $HSnPh_3$, respectively. When heated, two phenyl rings were cleaved from each of the two EPh_3 ligands, see Scheme 1.

These phenyl rings were combined with the four hydride ligands and were eliminated as benzene and the complexes **3** and **4** that contain square planar arrangements of the four ruthenium atoms with quadruply bridging EPh ligands on opposite sides of the Ru_4 plane were formed. A mechanism for the α-cleavage of a phenyl group from a $GePh_3$ ligand in a triiridium cluster complex has recently been established by a computational analysis [10].

We have also investigated the bonding and electronic transitions in **3** by computational analyses. It has been shown that the quadruply-bridging GePh ligands form delocalized bonding MOs to the $Ru_4(CO)_{12}$ cluster by using a_g and a_u combinations from two "σ-type" sp-hydrid orbitals and two b_g and two b_u orbitals by using unhybridized "π-like" p-orbitals on the two Ge atoms. The color observed for these complexes is due to symmetry-allowed electronic transitions in the Ru_4Ge_2 cluster core of the molecule.

Acknowledgments

This research was supported by the following grants from the National Science Foundation: CHE-1111496 to RDA and CHE-1048629 for the purchase of the computational facilities. We thank Dr. Xinzheng Yang at the University of California, Berkeley for helpful discussions.

Appendix A. Supplementary material

CCDC 891924–891926 contain the supplementary crystallographic data for this paper. These data can be obtained free of charge from The Cambridge Crystallographic Data Centre via www.ccdc.cam.ac.uk/data_request/cif.

References

[1] (a) R.D. Adams, E. Trufan, Phil. Trans. R. Soc. A 368 (2010) 1473;
(b) J.M. Thomas, B.F.G. Johnson, R. Raja, G. Sankar, P.A. Midgley, Acc. Chem. Res. 36 (2003) 20.(c) P. Braunstein, J. Rose, in: R.D. Adams, F.A. Cotton (Eds.), Catalysis by Di- and Polynuclear Metal Cluster Complexes, Wiley-VCH, New York, 1998 (Chapter 13);
(d) P. Braunstein, J. Rose, in: P. Braunstein, L.A. Oro, P.R. Raithby (Eds.), Metal Clusters In Chemistry, vol. 2, Wiley-VCH, Weinheim, 1999, pp. 616–677 (Chapter 2.2).
[2] (a) T. Ekou, A. Vicente, G. Lafaye, C. Especel, P. Marecot, Appl. Catal. A Gen. 314 (2006) 73;
(b) G. Lafaye, C. Micheaud-Especel, C. Montassier, Marecot, Appl. Catal. A Gen. 230 (2002) 19;
(c) G. Lafaye, C. Micheaud-Especel, C. Montassier, Marecot, Appl. Catal. A Gen. 257 (2004) 107.
[3] (a) R. Burch, J. Catal. 71 (1981) 348;
(b) R. Burch, L.C. Garla, J. Catal. 71 (1981) 360;
(c) R. Srinivasan, B.H. Davis, Platin. Met. Rev. 36 (1992) 151;
(d) T. Fujikawa, F.H. Ribeiro, G.A. Somorjai, J. Catal. 178 (1998) 58;
(e) Y.-K. Park, F.H. Ribeiro, G.A. Somorjai, J. Catal. 178 (1998) 66;
(f) F. Epron, C. Carnevillier, P. Marecot, Appl. Catal. 295 (2005) 157;
(g) R.D. Cortright, J. Dumesic, J. Catal. 148 (1994) 771;
(h) F.M. Dautzenberg, J.N. Helle, P. Biolen, W.M.H. Sachtler, J. Catal. 63 (1980) 119;
(i) G.W. Huber, J.W. Shabaker, J.A. Dumesic, Science 300 (2003) 2075;
(j) J.W. Shabaker, D.A. Simonetti, R.D. Cortright, J.A. Dumesic, J. Catal. 231 (2005) 67;
(k) M. Guidotti, V. Dal Aanto, A. Gallo, E. Gianotti, G. Peli, R. Psaro, L. Sordelli, Catal. Lett. 112 (2006) 89;
(l) R.D. Cortright, J.M. Hill, J.A. Dumesic, Catal. Today 55 (2000) 213;
(m) S. Hermans, R. Raja, J.M. Thomas, B.F.G. Johnson, G. Sankar, D. Gleeson, Angew. Chem. Int. Ed. 40 (2001) 1211;
(n) B.F.G. Johnson, S.A. Raynor, D.B. Brown, D.S. Shephard, T. Mashmeyer, J.M. Thomas, S. Hermans, R. Raja, G. Sankar, J. Mol. Catal. A Chem. 182–183 (2002) 89;
(o) S. Hermans, B.F.G. Johnson, Chem. Commun. (2000) 1955;
(p) R.D. Adams, D.A. Blom, B. Captain, R. Raja, J.M. Thomas, E. Trufan, Langmuir 24 (2008) 9223;
(q) R.D. Adams, E.M. Boswell, B. Captain, A.B. Hungria, P.A. Midgley, R. Raja, J.M. Thomas, Angew. Chem. Int. Ed. 46 (2007) 8182.
[4] (a) R.D. Adams, E.M. Boswell, B. Captain, M.A. Patel, Inorg. Chem. 46 (2007) 533;
(b) R.D. Adams, B. Captain, J.L. Smith Jr., Inorg. Chem. 44 (2005) 1413;
(c) R.D. Adams, B. Captain, E. Trufan, J. Cluster Sci. 18 (2007) 642.
[5] (a) F. Yang, E. Trufan, R.D. Adams, D.W. Goodman, J. Phys. Chem. C. 112 (2008) 14233–14235;
(b) R.D. Adams, B. Captain, E. Trufan, J. Organomet. Chem. 693 (2008) 3593–3602.
[6] (a) R.D. Adams, B. Captain, W. Fu, Inorg. Chem. 42 (2003) 1328–1333;
(b) R.D. Adams, B. Captain, W. Fu, M.D. Smith, Inorg. Chem. 41 (2002) 5593;
(c) R.D. Adams, B. Captain, W. Fu, M.D. Smith, Inorg. Chem. 41 (2002) 2302.
[7] R.D. Adams, B. Captain, J.L. Smith Jr., M.B. Hall, C.L. Beddie, C.E. Webster, Inorg. Chem. 43 (2004) 7576.
[8] R.D. Adams, B. Captain, R.H. Herber, M. Johansson, I. Nowik, J.L. Smith Jr., M.D. Smith, Inorg. Chem. 44 (2005) 6346.
[9] R.D. Adams, Y. Kan, Q. Zhang, Organometallics 30 (2011) 328.
[10] R.D. Adams, F. Fang, Q. Zhang, M.B. Hall, E. Trufan, Organometallics 31 (2012) 2621.
[11] (a) S.E. Anema, S.K. Lee, K.M. Mackay, L.C. McLoed, B.K. Nickolson, J. Chem. Soc. Dalton Trans. (1991) 1209;
(b) S.E. Anema, S.K. Lee, K.M. Mackay, B.K. Nickolson, M. Service, J. Chem. Soc. Dalton Trans. (1991) 1201;
(c) S.K. Lee, K.M. Mackay, B.K. Nickolson, J. Chem. Soc. Dalton Trans. (1993) 715;
(d) S.P. Foster, K.M. Mackay, B.K. Nickolson, J. Chem. Soc. Chem. Commun. (1982) 1156;
(e) P. Gusbeth, H. Vahrenkamp, Chem. Ber. 118 (1985) 1747.
[12] C.R. Eady, B.F.G. Johnson, J. Lewis, J. Chem. Soc. Dalton Trans. (1977) 477.
[13] R.D. Adams, B. Captain, M.B. Hall, E. Trufan, X. Yang, J. Am. Chem. Soc. 129 (2007) 12328.
[14] SAINT+, Version 6.2a, Bruker Analytical X-ray Systems, Inc., Madison, WI, 2001.
[15] G.M. Sheldrick, SHELXTL, Version 6.1, Bruker Analytical X-ray Systems, Inc, Madison, WI, 1997.
[16] (a) G. te Velde, F.M. Bickelhaupt, S.J.A van Gisbergen, C. Fonseca Guerra, E.J. Baerends, J.G. Snijders, T. Ziegler, Chemistry with ADF, J. Comp. Chem. 22 (2001) 931;
(b) C. Fonseca Guerra, J.G. Snijders, G. te Velde, E.J. Baerends, Towards an order-N DFT method, Theoret. Chem. Accts. 99 (1998) 391;
(c) J.P. Perdew, A. Ruzsinszky, G.I. Csonka, O.A. Vydrov, G.E. Scuseria, Phys. Rev. Lett. 100 (2008) 136406.
[17] (a) R. Bau, M.H. Drabnis, Inorg. Chim. Acta 259 (1997) 27;
(b) R.G. Teller, R. Bau, Struc. Bonding 41 (1981) 1.
[18] J. Lauher, J. Am. Chem. Soc. 100 (1978) 5305.
[19] B.H.S. Thimmappa, J. Cluster Sci. 7 (1996) 1.
[20] J.-F. Halet, R. Hoffmann, J.-Y. Saillard, Inorg. Chem. 24 (1985) 1695.